Comprehensive Three-Dimensional Dynamic Modeling of Liquid Crystal Devices Using Finite Element Method

Zhibing Ge, *Student Member, IEEE*, Thomas X. Wu, *Senior Member, IEEE*, Ruibo Lu, Xinyu Zhu, Qi Hong, and Shin-Tson Wu, *Fellow, IEEE*

***Abstract*—In this paper, a comprehensive open-source three-dimensional (3-D) finite-element method (FEM) is proposed to model the dynamic behavior of liquid crystal (LC) directors in complex structures. This dynamic model is based on interactively iterating the vector representation of director profile and potential distribution. The director update formulations are derived in detail from the Galerkin's approach of FEM, including the weak form approach to simplify the highly nonlinear iteration equation. The potential update formulations are derived from the Ritz's approach of FEM. A 2-D in-plane switching (IPS) structure is used as an example to compare our approach with the FEM based commercial software (2dimMOS). The results from both programs show an excellent agreement. Furthermore, our method also agrees well with the finite-difference method (FDM) in studying a 3-D super IPS LC cell with zigzag electrodes.**

***Index Terms*—Liquid crystal devices, liquid crystal displays, modeling, finite element method.**

I. Introduction

LIQUID CRYSTAL (LC) materials have been used widely in direct-view and projection displays. Accurate and reliable modeling of LC electro-optic behaviors is critical in both developing novel devices and optimizing the current display devices. Generally, the LC modeling includes two steps: evaluation of the LC directors' deformation under external electric fields and calculation of the optical properties thereafter. Therefore, an accurate model of LC deformation is a prerequisite for reliable device design and subsequent optical analysis. In general, the dynamic modeling of the LC director calculations can be implemented by finite-difference method (FDM) [1], [2], finite-element method (FEM) [3], [4], or a combination of both. The success of these methods in accurate modeling of LC devices has been demonstrated by the development of LC modeling software, such as LC3D [2], DIMOS [5], LCD Master [6], Techwitz LCD [7], LCD-DESIGN [8], LCQuest [9], and others.

Several factors make FEM a strong contender for modeling LC devices. The primary reason is that FEM is versatile in modeling arbitrary LC device structures with adaptive meshing technique. Further, as a direct solver (seeking solutions via directly solving linear system problems) in contrast to FDM (seeking solutions via iterations) [1]–[4], this method can generate accurate solutions from solving large sparse matrix system, which is an inherent property of FEM. Since efficient algorithms for large sparse matrix system in other areas such as mathematics, mechanics, and electromagnetics are well developed, they can be introduced to the LC device modeling without much extra effort. In addition, the development of computer aided symbolic derivation techniques nowadays makes automatic FEM formula generation in LC modeling possible, which was previously the main obstacle to introduce FEM into accurate LC simulations. Several papers have already exploited the FEM in the study of advanced LC devices [10]–[16]. However, their focus is more device physics oriented. To the best of our knowledge, no literature has ever reported an open-source comprehensive mathematical derivation and formulation of the FEM in LCD modeling. The lack of this part in LCD simulators has hindered the research as well as applications of LCD technologies. Therefore, the main objective of this paper is to propose a comprehensive dynamic modeling of LC deformations by FEM, which includes a detailed derivation of the FEM formulations. In addition, a special technique, the weak form method [3], [4] to greatly simplify formula derivations, is introduced as well.

In this paper, we first introduce the derivation of update equations for LC director and potential profiles, as well as the iteration scheme for the LC dynamics. Then, FEM is employed to solve the above derived highly nonlinear equations based on the Galerkin's method [3], [4] for director profile and Ritz's method [3], [4] for potential profile. Derivations of the nonlinear update equations show that the highest spatial derivative is in the second order (e.g., $(\partial^2/\partial x \partial y)$). Therefore, we introduce the weak form method [3], [4] to simplify the director update equations. This technique makes the first-order 3-D FEM interpolation function (tetrahedron shaped) accurate enough. Furthermore, some effects which influence the director distribution such as surface anchoring and flexoelectric polarization [17], [18] are discussed as well. To verify our derivations, a 2-D in-plane-switching (IPS) structure [19] is then studied by the above-derived method and the FEM-based 2dimMOS [5]. Finally, a 3-D super IPS structure with zigzag electrodes [20] is simulated using our FEM and results are compared to those derived from FDM to validate our derivations as well.

Manuscript received June 6, 2005; revised July 24, 2005. This work is supported by Toppoly Optoelectronics Corporation (Taiwan), Taiwan, R.O.C.

Z. Ge, T. X. Wu, and Q. Hong are with the Department of Electrical and Computer Engineering, University of Central Florida, Orlando, FL 32816 USA (e-mail: zge@mail.ucf.edu; tomwu@mail.ucf.edu; qhong@creol.ucf.edu).

R. Lu, X. Zhu, and S.-T. Wu are with the College of Optics and Photonics, University of Central Florida, Orlando, FL 32816 USA (e-mail: rlu@creol.ucf.edu; xzhu@creol.ucf.edu; swu@creol.ucf.edu).

Digital Object Identifier 10.1109/JDT.2005.858885

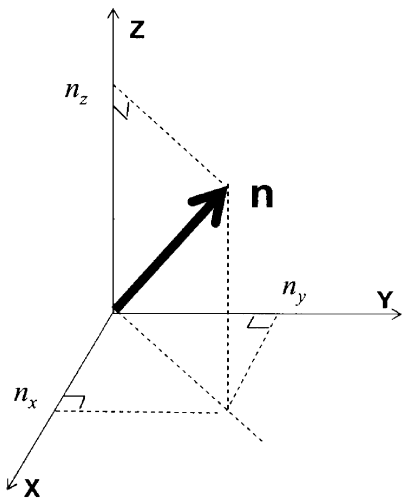

Fig. 1. Vector representation of a LC director.

II. Mathematical Formulations

A. Dynamic Model of LC Devices

Modeling of the dynamics of LC directors in response to external voltages generally starts off with minimizing the LC free energy within the LC cell [21], [22]. However, owing to the high nonlinearity of the free energy expressions and the coupling between elastic and electric energies, a direct solution of the LC director deformation and potential distribution from the free energy equation is almost impossible. Therefore, the dynamic modeling usually involves an iteration process [2]: minimizing the LC free energy to update the LC director profile and solving the Gauss law (or minimizing the electric energy) to update the potential profile interactively. In modeling the LC directors, both vector representation [23], as shown in Fig. 1, and Q tensor [24]–[26] methods can be employed. Detailed comparison of these two methods is provided in [2]. Owing to its mathematical simplicity, fast computing speed, and reliability, the vector method is widely employed in LCD simulations. In this paper, we refer the vector method in our derivations.

1) Director Profile Update Theory: Numerical simulation of LC transient state at each time step under constant voltage is based on minimizing Gibbs free energy [21], [22], which is the difference between Frank-Oseen strain free energy [18], [27], [28] and electric energy, by solving the Euler Lagrange equation [2], [22]. The Gibbs free energy density in the LC cell can be expressed as

$$f = \frac{1}{2}K_{11}(\nabla \cdot \mathbf{n})^2 + \frac{1}{2}K_{22}(\mathbf{n} \cdot \nabla \times \mathbf{n} + q_0)^2 + \frac{1}{2}K_{33}|\mathbf{n} \times \nabla \times \mathbf{n}|^2 - \frac{1}{2}\mathbf{D} \cdot \mathbf{E} \quad (1)$$

where

$$\mathbf{D} = \varepsilon_0 \overleftrightarrow{\varepsilon}\mathbf{E} \quad (2)$$

$$\mathbf{E} = -\nabla\Phi \quad (3)$$

and $\mathbf{n} = (n_x, n_y, n_z)$ is the unit vector form of LC directors in the given coordinates, as shown in Fig. 1; q_0 is the chiral wavenumber, which is a parameter specifying the equilibrium twist state of the LC; K_{11}, K_{22}, and K_{33} are the elastic constants of the LC materials; and $\mathbf{D}, \mathbf{E}, \Phi$ are the electric displacement, electric field, and potential function in the entire system region, respectively; $\overleftrightarrow{\varepsilon}$ is the dielectric tensor of LC material which correlates $\mathbf{D}$ and $\mathbf{E}$. It is known that to minimize the system free energy (a volume integral of the energy density) by solving Euler–Lagrange equation with inclusion of a Rayleigh dissipation function will result in [2], [22]

$$\gamma\frac{dn_l}{dt} = -\left(\frac{\partial f}{\partial n_l} - \frac{d}{dx}\frac{\partial f}{\partial(dn_l/dx)} - \frac{d}{dy}\frac{\partial f}{\partial(dn_l/dy)} - \frac{d}{dz}\frac{\partial f}{\partial(dn_l/dz)}\right) + \lambda n_l \quad (4)$$

where n_l represents n_x, n_y, and n_z, and λ is a Lagrange multiplier to constrain the unit length of the director n_l (i.e., $n_x^2 + n_y^2 + n_z^2 = 1$). Here the fluid flow effect is assumed to have secondary importance and is thus ignored in (4). The Lagrange multiplier λ can be further dropped, if the calculated n_x, n_y, and n_z is normalized as $n_i = (n_i/\sqrt{n_x^2 + n_y^2 + n_z^2})(i = x, y, z)$ at each iteration step. Therefore, (4) specifying the iterative relation of LC directors under external applied voltages can be further simplified to the following form:

$$\frac{dn_l}{dt} + \frac{1}{\gamma}[f]_{n_l} = 0 \quad (l = x, y, z) \quad (5)$$

where

$$[f]_{n_l} = \left(\frac{\partial f}{\partial n_l} - \frac{d}{dx}\frac{\partial f}{\partial(dn_l/dx)} - \frac{d}{dy}\frac{\partial f}{\partial(dn_l/dy)} - \frac{d}{dz}\frac{\partial f}{\partial(dn_l/dz)}\right). \quad (6)$$

By taking a time-difference $(dn_l/dt) = (n_l^{t+\Delta t} - n_l^t/\Delta t)$, (5) can be further expressed as

$$n_l^{t+\Delta t} = n_l^t - \frac{\Delta t}{\gamma}[f]_{n_l} \quad (l = x, y, z). \quad (7)$$

Since the dielectric tensor $\overleftrightarrow{\varepsilon}$ includes the LC director $\mathbf{n} = (n_x, n_y, n_z)$, the potential and the director functions in $[f]_{n_l}$ are coupled with each other as indicated by (1)–(3). Computer assisted derivations show $[f]_{n_l}$ has a highly nonlinear form containing the highest spatial derivative of n_l with respect to x, y, and z up to the second order (e.g., $(\partial^2 n_l/\partial x \partial y)$). In order to use the first order 3D tetrahedral basis function to evaluate these second order derivatives, weak form method is introduced, as will be discussed in later sections.

2) Potential Profile Update Theory: At given LC director distribution and electrode voltage, the potential profile Φ can be determined by solving the Gauss law

$$\nabla \cdot \mathbf{D} = 0. \quad (8)$$

The displacement $\mathbf{D}$ is expressed in terms of the potential Φ as indicated in (2) and (3). Here solving the above equation is equivalent to minimizing the electric energy $F_e = \int_\Omega (1/2)\mathbf{D} \cdot \mathbf{E}\, d\Omega$ in the bulk from the variational aspect. The bulk region defined here includes the LC cell and other regions, such as the substrates. Both direct solver (e.g., FEM with Ritz's method or Galerkin's method) and iterative approach (e.g., FDM with iterations) can be employed to solve the desired potential distribution. Due to the simplicity in implementation and the inherited accuracy of direct solver, we will take FEM with Ritz's method in the following derivations.

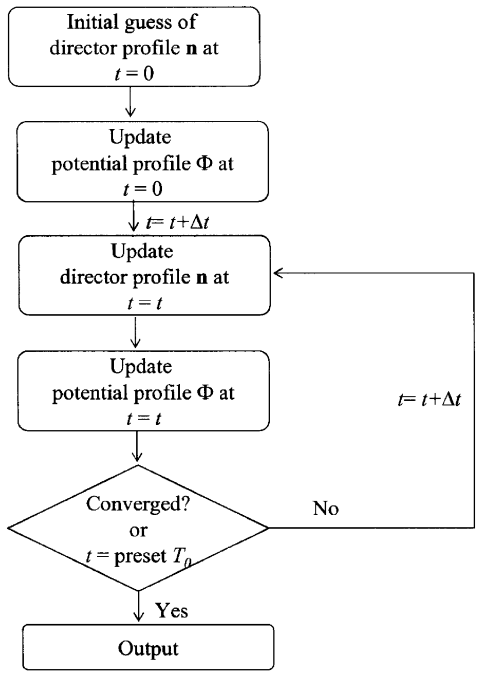

Fig. 2. Iteration flowchart of the dynamic modeling.

3) Modeling Flowchart: As explained in Sections II-A1 and II-A2, the coupling between director deformations and applied electric fields makes it almost impossible to obtain both director and potential profile solutions simultaneously. However, this challenge can be overcome by the iteration approach. A detailed iterative scheme is illustrated in Fig. 2. The initial LC director profile can usually be preset by its boundary conditions. The stability of this iterative updating scheme is an important issue [29], which relies on a proper selection of updating time step Δt in (7).

B. FEM Implementation

The solution for the above-mentioned iteration scheme includes two iterative steps: 1) solving the potential distribution at a given director profile and 2) solving the director profile at a given potential distribution. FEM is employed to solve these iteration formulations.

1) Director Update Formulations via Galerkin's Method: The high nonlinearity of (1) indicates that direct solution of the LC director distribution is difficult to obtain. However, Galerkin's method can bypass this difficulty. The Galerkin's method belongs to the family of weighted residual methods, which seek the solution by weighting the residual of the differential equations. Suppose we divide the study region Ω into M element regions with N nodes (considering the first order interpolation function). The local element has a specific shape, such as a tetrahedral block in the 3-D FEM case. The general solution of each director component n_x, n_y, or n_z can be approximated by interpolating from its values on the N global nodes using global interpolation functions as

$$\tilde{n}_l = \sum_{j=1}^{N} n_{l,j} W_j \quad (l = x, y, z) \tag{9}$$

where $\tilde{n}_l$ is the approximate solution of $n_l \cdot n_{l,j}$ and W_j are the jth node value of and interpolation function in the entire region, respectively. The specific form of W_j will be discussed later in this paper. After inserting $\tilde{n}_l$ into (5), the residual R, error of the interpolation, can be written as

$$R = \frac{d\tilde{n}_l}{dt} + \frac{1}{\gamma}[f]_{\tilde{n}_l} \quad (l = x, y, z). \tag{10}$$

The exact solution occurs only when R equals 0. Due to the above approximation, the residual R always leads to a nonzero value. However, with Galerkin's method, the residual R can be minimized through weighting the residual R by interpolation function W_i as

$$\int_{\Omega} \left(\frac{d\tilde{n}_l}{dt} + \frac{1}{\gamma}[f]_{\tilde{n}_l} \right) W_i \, d\Omega = 0, \quad (i = 1, 2, \ldots N \text{ and } l = x, y, z). \tag{11}$$

Here, $\int_{\Omega} d\Omega$ denotes the integral on the study domain Ω, which can be 1-D to 3-D integrals for different problems. Replacing the $\tilde{n}_l$ here by (9) yields

$$\sum_{j=1}^{N} \left(\int_{\Omega} W_i W_j d\Omega \right) \frac{dn_{l,j}}{dt} = -\int_{\Omega} \frac{1}{\gamma}[f]_{\tilde{n}_l} W_i d\Omega \quad (i = 1, 2, \ldots N \text{ and } l = x, y, z). \tag{12}$$

For each $n_l (l = x, y, z)$, we can obtain N linear equations with N variables $n_{l,j}$. This equation group can be written in a matrix representation as

$$[A](dn_l/dt) = (b) \quad (l = x, y, z) \tag{13}$$

where [ ] denotes a matrix and ( ) denotes a vector, with

$$A_{i,j} = \int_{\Omega} W_i W_j d\Omega, \tag{14}$$

$$b_i = -\int_{\Omega} \frac{1}{\gamma}[f]_{\tilde{n}_l} / W_i d\Omega. \tag{15}$$

By taking the same forward time-difference scheme $(dn_l/dt) = (n_l^{t+\Delta t} - n_l^t/\Delta t)$ as (7), we can obtain the iteration relation via Galerkin's method in a matrix representation as

$$\left(n_l^{t+\Delta t}\right) = \left(n_l^t\right) + \Delta t [A]^{-1} (b) \quad (l = x, y, z). \tag{16}$$

Equation (16) is the final iteration equation of the dynamic model, which specifies the director profile correlation between two consecutive time steps.

However, the above-mentioned matrix A and vector b is still not easy to obtain because a good group of interpolation function W defined on the entire domain is difficult to assign. Here FEM can automatically generate an appropriate group of interpolation functions. The detailed derivation with FEM in obtaining the matrix A and vector b is provided in Appendix A.

The advantage of this method is evident that the global matrix A in (13) is uniquely determined by the mesh and the interpolation functions, as indicated in (A-5) in the Appendix A. As a result, in updating director profiles from (16), the matrix

A only needs to be calculated at the first iteration step and can then be stored for subsequent iteration steps. Utilizing this property greatly reduces the computing time in the director updating procedure.

2) Potential Update Formulations via Ritz's Method: From the analysis of the potential update theory, the update of potential is equivalent to solve the Gaussian law of (8), or minimizing the system electric energy $F_e = \int_\Omega (1/2)\mathbf{D}\cdot\mathbf{E}d\Omega$ from a variational viewpoint. In our derivations, we use the Ritz's method to minimize the system electric energy, which inherits a more apparent physical and mathematical meaning than to apply Galerkin's method in solving the Gaussian law.

The free electric energy F_e in the study domain is equal to

$$F_e = \int_\Omega \frac{1}{2}\mathbf{D}\cdot\mathbf{E}d\Omega = \int_\Omega \frac{1}{2}\varepsilon_0(\overleftrightarrow{\varepsilon}\nabla\Phi)\cdot(\nabla\Phi)d\Omega. \tag{17}$$

Here $\overleftrightarrow{\varepsilon}$ is a tensor for anisotropic media, such as the LC layer, and a scalar for isotropic media, such as the glass substrates. Similarly, the approximate global potential solution $\tilde{\Phi}$ can be expressed by the global node value Φ_j and global interpolation function W_j as

$$\tilde{\Phi} = \sum_{j=1}^{N}\Phi_j W_j. \tag{18}$$

Thus, F_e is a function of N global variables $\Phi_j (j = 1,2,\dots N)$, here N might be different with the total node number in the director update. From mathematical theory, its value is minimized where the relative partial derivative of F_e with respect to Φ_j equals zero. This leads to N equations as

$$\frac{\partial F_e}{\partial \Phi_j} = 0, \qquad j = 1,2,\dots N. \tag{19}$$

This equation group can be further expressed as a matrix representation

$$[B](\Phi) = (0). \tag{20}$$

Again, here [ ] denotes a matrix and ( ) denotes a vector. Each element in matrix B has a form of

$$\begin{aligned} B_{i,j} &= \frac{\partial^2 F_e}{\partial\Phi_i\partial\Phi_j} \\ &= \frac{1}{2}\varepsilon_0\int_\Omega\left(\frac{\partial W_i}{\partial x},\frac{\partial W_i}{\partial y},\frac{\partial W_i}{\partial z}\right) \\ &\quad\times\left(\overleftrightarrow{\varepsilon}\left(\frac{\partial W_j}{\partial x},\frac{\partial W_j}{\partial y},\frac{\partial W_j}{\partial z}\right)^T\right)d\Omega \\ &\quad+\frac{1}{2}\varepsilon_0\int_\Omega\left(\frac{\partial W_j}{\partial x},\frac{\partial W_j}{\partial y},\frac{\partial W_j}{\partial z}\right) \\ &\quad\times\left(\overleftrightarrow{\varepsilon}\left(\frac{\partial W_i}{\partial x},\frac{\partial W_i}{\partial y},\frac{\partial W_i}{\partial z}\right)^T\right)d\Omega. \end{aligned} \tag{21}$$

The detailed derivation of $B_{i,j}$ and further implementation by FEM is described in Appendix B. Here for the nematic LC material, the tensor $\overleftrightarrow{\varepsilon}$ is a symmetric matrix. This symmetric property can further simplify $B_{i,j}$ to the following form:

$$\begin{aligned} B_{i,j} = \varepsilon_0\int_\Omega&\left(\frac{\partial W_i}{\partial x},\frac{\partial W_i}{\partial y},\frac{\partial W_i}{\partial z}\right) \\ &\times\left(\overleftrightarrow{\varepsilon}\left(\frac{\partial W_j}{\partial x},\frac{\partial W_j}{\partial y},\frac{\partial W_j}{\partial z}\right)^T\right)d\Omega. \end{aligned} \tag{22}$$

3) Weak Form Technique: As explained in above sections, the matrix A, B for director and potential calculations have definite forms and can be directly obtained from their corresponding equations using FEM. Still, the difficulty lies in the complicated derivations of global vector b in (15). Although approximation of the derivations can be applied [12], its accuracy in some complex device structures is not always guaranteed. Therefore, the state-of-the-art computer software such as MAPLE [30] is used to generate FEM-based formulation derivations. We find the highest order of spatial derivative of n_l with respect to x, y, and z is up to the second order. As a result, the first order of interpolation/basis function [e.g., (A-2)] will lose accuracy due to the fact that its second order spatial derivative equals to zero. For example, let us assume there is one term $\iiint_{\Omega_e}\beta(\partial^2 n_l^e/\partial x\partial z)W_i^e dx\,dy\,dz$ in b_i^e, as shown in (A-6). After substituting $\tilde{n}_l^e = \sum_{j=1}^m n_{l,j}^e W_j^e$ into b_i^e with the first order interpolation function W_j^e, the second order derivative $(\partial^2 n_l^e/\partial x\partial z)$ diminishes to zero, which does not always hold.

A good solution of this issue is to introduce the weak form method. Derivations of (6) based on commercial software show that $[f]_{n_l}$ can be summarized into a general expression

$$[f]_{n_l} = [f_0]_{n_l} + \sum f_{i,j,k}^l\frac{\partial^2 n_i}{\partial j\partial k} \quad (l,i,j,k = x,y,z). \tag{23}$$

where $[f_0]_{n_l}$ stands for the terms with highest derivatives up to the first order, $f_{i,j,k}^l(\partial^2 n_i/\partial j\partial k)$ denotes these second order derivative terms (e.g., $f_{z,x,x}^l(\partial^2 n_z/\partial x\partial x)$) with $f_{i,j,k}^l$ as the coefficient. Neglecting the subscript index i, we now rewrite (15) in the following form as

$$b = -\frac{1}{\gamma}\int\int\int_{x,y,z}[f]_{n_l}W\,dx\,dy\,dz. \tag{24}$$

Substituting $[f]_{n_l}$ from (23) into (24) yields

$$\begin{aligned} b = -\frac{1}{\gamma}\Bigg(&\int\int\int_{x,y,z}[f_0]_{n_l}W\,dx\,dy\,dz \\ &+\int\int\int_{x,y,z}\sum f_{i,j,k}^l\frac{\partial^2 n_i}{\partial j\partial k}W\,dx\,dy\,dz\Bigg) \\ &(l,i,j,k = x,y,z). \end{aligned} \tag{25}$$

In (25), the first term with derivatives up to first order can be accurately calculated by FEM with first-order interpolation function W. Although there are many terms with second-order derivatives, they can always be divided into two categories: 1)

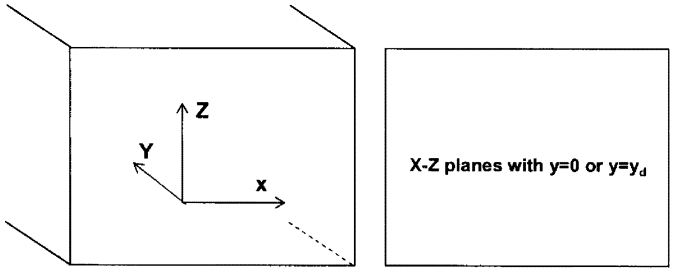

Fig. 3. 2-D boundary planes from a 3-D bulk.

either j or k equals to z and 2) neither j nor k equals to z. As an illustration of taking the weak form to accurately evaluate these terms in (25), we just select two typical terms belonging to these two categories: 1) $\iint\limits_{x,y,z} f^l_{x,y,z}(\partial^2 n_x/\partial y\partial z)W\,dx\,dy\,dz$, and 2) $\iint\limits_{x,y,z} f^l_{z,x,y}(\partial^2 n_z/\partial x\partial y)W\,dx\,dy\,dz$. Using the integration by parts, we obtain

$$\begin{aligned}
&\iiint\limits_{x,y,z} f^l_{x,y,z}\frac{\partial^2 n_x}{\partial y\partial z}W\,dx\,dy\,dz\\
&\quad=-\iiint\limits_{x,y,z}\frac{\partial n_x}{\partial y}\frac{\partial\left(f^l_{x,y,z}W\right)}{\partial z}dx\,dy\,dz\\
&\qquad+\iint\limits_{x,y}\left(\frac{\partial n_x}{\partial y}f^l_{x,y,z}W\right)\Bigg|_{z=0}^{z=z_d}dx\,dy \qquad (26)\\
&\iiint\limits_{x,y,z} f^l_{z,x,y}\frac{\partial^2 n_z}{\partial x\partial y}W\,dx\,dy\,dz\\
&\quad=-\iiint\limits_{x,y,z}\frac{\partial n_z}{\partial x}\frac{\partial\left(f^l_{z,x,y}W\right)}{\partial y}dx\,dy\,dz\\
&\qquad+\iint\limits_{x,z}\left(\frac{\partial n_z}{\partial x}f^l_{z,x,y}W\right)\Bigg|_{y=0}^{y=y_d}dxdz \qquad (27)
\end{aligned}$$

where z_d and y_d denote the boundary coordinates in the vertical z and lateral y directions. Because the director $\mathbf{n}=(n_x,n_y,n_z)$ is fixed under strong anchoring assumption in the vertical z direction, i.e., $(\partial n^e_l/\partial i)=0(i=x,y,z)$ at these boundaries, the 2-D integral term in (26) equals zero. This property further simplifies (26) into

$$\begin{aligned}
&\iiint\limits_{x,y,z} f^l_{x,y,z}\frac{\partial^2 n_x}{\partial y\partial z}W\,dx\,dy\,dz\\
&\qquad=-\iiint\limits_{x,y,z}\frac{\partial n_x}{\partial y}\frac{\partial\left(f^l_{x,y,z}W\right)}{\partial z}dx\,dy\,dz \qquad (28)
\end{aligned}$$

which makes $\iint\limits_{x,y,z} f^l_{x,y,z}(\partial^2 n_x/\partial y\partial z)W\,dx\,dy\,dz$ calculable by the first-order interpolation functions. On the other hand, the 2-D integral term $\int\int\limits_{x,z}((\partial n_z/\partial x)f^l_{z,x,y}W)|_{y=0}^{y=y_d}dx\,dz$ in (27) is not always equal to zero on the boundaries in the y direction. However, as illustrated in Fig. 3, the term

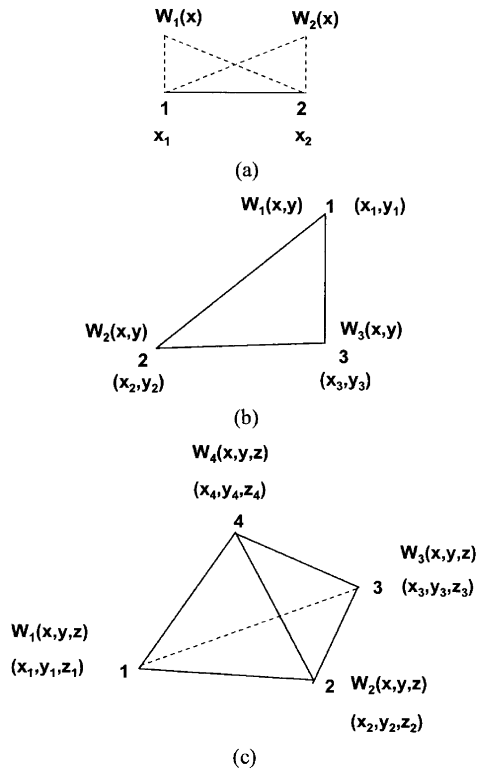

Fig. 4. (a) 1-D interpolation function. (b) 2-D interpolation function. (c) 3-D interpolation function.

$\int\int\limits_{x,z}((\partial n_z/\partial x)f^l_{z,x,y}W)|_{y=0}^{y=y_d}\,dx\,dz$ in (27) can be further expressed on $y=0$ and $y=y_d$ planes by

$$\begin{aligned}
&\iint\limits_{x,z}\left(\frac{\partial n_z}{\partial x}f^l_{z,x,y}W\right)\Bigg|_{y=0}^{y=y_d}dx\,dz\\
&\quad=\iint\limits_{x,z}\left(\frac{\partial n_z}{\partial x}f^l_{z,x,y}W(x,y=y_d,z)\right)dx\,dz\\
&\qquad-\iint\limits_{x,z}\left(\frac{\partial n_z}{\partial x}f^l_{z,x,y}W(x,y=0,z)\right)dx\,dz. \qquad (29)
\end{aligned}$$

The 3-D interpolation function $W(x,y,z)$ decays to a 2-D interpolation function on the boundary planes ($x-z$ plane at $y=0$ and $y=y_d$ in this case), as shown in Fig. 4(b) and (c). To evaluate this term, we can use 2-D FEM on the lateral boundary planes to calculate (29). This is equivalent to weight $(\partial n_z/\partial x)f^l_{z,x,y}$ by 2-D FEM with 2-D interpolation functions generated from $W(x,y,z)$ on the boundary planes (x-z plane at $y=0$ and $y=y_d$ in this case). The lateral derivative terms in x and y directions (e. g., $(\partial n_z/\partial x)$) can be calculated by a finite difference from the boundary point and its adjacent ones (e.g., $(\partial n_z/\partial x)|_{x=0}=(n_z(x=\Delta x)-n_z(x=0)/\Delta x)$). With the assistance of FEM, these 2-D integral terms are calculable and can be added to the 3-D integral terms evaluated by first order interpolation functions. Other second order terms in (25) can be calculated similarly in the same way as (26)–(29).

In other words, by taking the weak form method into derivations of (25), these second-order derivative terms will degrade one order, which can be calculated by using the first-order

interpolation functions. Therefore, introducing the weak form greatly facilitates the derivation of vector b without any further approximations to sacrifice simulation accuracy.

4) Boundary Conditions and Other Topics: In solving the LC director and potential profiles, their boundary conditions in the study cell need to be well-defined. As shown in Fig. 5, typical potential boundary conditions on electrodes are the Dirichlet boundary conditions, i.e., the potential values on electrodes 1 and 2 are fixed to assigned voltages. In the far regions along the z direction, such as the outer boundaries of the supporting substrates where no electrodes are present, the Neumann conditions apply to the potential, i.e., the spatial normal derivative of potential (e.g., $(\partial\Phi/\partial z)$) equals zero. In the implementation of these boundary conditions for the potential, the fixed values on the electrodes can be forced by matrix and vector manipulation in (20), and the Neumann condition for potential in the far regions are naturally satisfied in FEM with the assumption that the electric energy is totally confined in the LC cells as well as the substrate regions.

For the LC director calculations, in the vertical z direction, the director $\mathbf{n} = (n_x, n_y, n_z)$ on the top and bottom alignment layer—LC interfaces (at $z = 0$ and $z = z_d$) are usually specified by initial pretilt and azimuthal angle values. With strong anchoring assumption, the director values on these interfaces are fixed. A more general case is to take the surface anchoring energy into consideration. The surface anchoring energy density from the Rapini-Papoular model [31], [32] on the vertical boundaries has the following forms:

$$f_s = \frac{1}{2}C_\theta \sin^2(\theta - \theta_r) + \frac{1}{2}C_\Phi \sin^2(\Phi - \Phi_r) \qquad (30)$$

where C_θ and C_Φ are the polar and azimuthal anchoring energy coefficients (J/m^2), θ_r and Φ_r are the pretilt polar angle and twist angle, respectively. Equation (30) can be expanded and expressed in terms of the director components n_x, n_y and n_z as

$$\begin{aligned} f_s = {} & \frac{1}{2}C_\theta \left[n_z^2 \cos^2\theta_r + \left(1 - n_z^2\right)\sin^2\theta_r \right. \\ & \left. - n_z\sqrt{1-n_z^2}\sin 2\theta_r \right] + \frac{1}{2}C_\Phi \left[\frac{n_y^2}{1-n_z^2}\cos^2\Phi_r \right. \\ & \left. + \frac{n_x^2}{1-n_z^2}\sin^2\Phi_r - \frac{n_x n_y}{1-n_z^2}\sin 2\Phi_r \right]. \end{aligned} \qquad (31)$$

The surface anchoring energy from above density function can be added to the total Gibbs free energy integrated from (1). Here, one needs to beware the difference in unit between the surface anchoring energy density (J/m ^{2}) and the bulk Gibbs energy density (J/m ^{3}). In the lateral direction (x, y direction), $\mathbf{n} = (n_x, n_y, n_z)$ can be determined by Dirichlet boundary conditions, i.e., the $\mathbf{n} = (n_x, n_y, n_z)$ values are fixed, or by Neumann conditions, i.e., $(\partial n_l^e/\partial i) = 0 (i, l = x, y, z)$ at lateral boundary planes, which is determined by specific device configurations. Another type of lateral boundary condition frequently employed in LCD simulation is the periodic boundary condition. The director $\mathbf{n} = (n_x, n_y, n_z)$ and its derivatives have equal values at two later periodic boundaries, such as planes at $x = 0$ and $x = x_d$ in Fig. 5. Because the LC cell patterns in the pixel are usually periodically repeated in some devices such as in the IPS mode, the calculation results from one period are enough to represent the entire pixel. The periodic boundary condition greatly reduces the computing load in simulating large size pixels with periodic configurations.

Those abovementioned boundary conditions are most widely employed in the LC device simulations. However, boundary conditions for the potential and director update are not confined to these categories. In stead, they need to be designated in accordance to the specific problems studied.

In addition to the inclusion of surface anchoring energy, flexoelectric polarization [17], [18] is another important effect that needs to be considered under certain conditions. Flexoelectric effect describes the spontaneous polarization generated by a deformation of the director in nematic phase composed of molecules, which exhibit shape asymmetry and have permanent dipole moments. The flexoelectricity induced polarization will interact with the applied electric fields and deform the LC directors. A phenomenological expression for this polarization is given by $\mathbf{P} = e_s\mathbf{n}(\nabla\cdot\mathbf{n}) + e_b\mathbf{n}\times(\nabla\times\mathbf{n})$ [33]. Here e_s and e_b are the splay and bend flexoelectric coefficients. The coupling of this polarization with electric fields and LC deformations will introduce an additional term to the Gibbs free energy density in (1) as $-\mathbf{P}\cdot\mathbf{E}$, thus it can be counted by the FEM as described in above sections as well. Detailed introduction and discussion of the flexoelectric effect in LC modeling can be found in [17], [18], [33]–[38], and references therein.

Other effects that might affect the deformations LC directors and potential distributions in a cell under certain conditions can be referred to detailed discussion in the [39].

III. Results and Discussion

To illustrate and validate the FEM-based LC dynamic modeling with the above derived formulations, we use a 2-D interdigital IPS structure with rectangular electrodes as an example to compare our own developed method with the FEM-based commercial software 2dimMOS. In addition, we use a 3-D super IPS with zigzag electrodes to compare our method with the FDM.

A. Two-Dimensional Conventional IPS Structure

Fig. 5 depicts a conventional 2-D IPS structure. The LC material employed is MLC-6692 (from Merck) with its parameters listed as follows: $n_e = 1.5644, n_o = 1.4794, \varepsilon_{//} = 14.2, \varepsilon_\perp = 4.2, K_{11} = 9.6$ pN, $K_{22} = 6.1$ pN, $K_{33} = 14.1$ pN, and rotational viscosity $\gamma_1 = 0.1$ Pa $\cdot$ s. The LC cell gap is 4 μm, the LC pretilt angles on both substrates are 2°, and the rubbing angles are 80° away from the x axis in the $x - y$ plane. In Fig. 5, the electrodes 1 and 2 are located in the same bottom planes at $z = 0$, with an equal length of 4 μm and a separation distance of 8 μm.

In the simulation, the electrode 1 is applied with 6 V, and the electrode 2 is grounded. The LC directors on the vertical boundaries are assumed to be strongly anchored in our simulations. The x direction periodic boundary conditions in Fig. 5 are applied to both potential and LC director calculations. In the 2dimMOS, since no periodic boundary conditions are available,

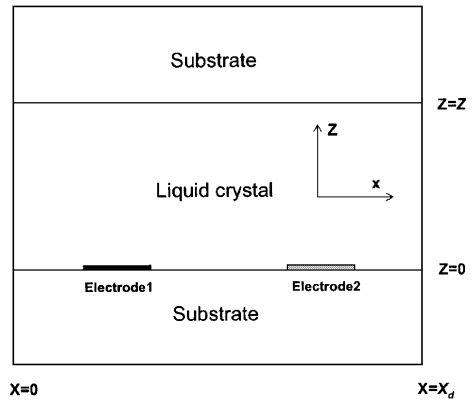

Fig. 5. A conventional 2-D in-plane switching structures.

we just expand two more periods in both left and right x directions to approximate the periodicity in the 2dimMOS (a total of five periods). Here we take the center-truncated region (one period) from the 2dimMOS to compare with our simulation based on the derived method in Section II.

Fig. 6(a) and (b) plot the director distribution at 4 and 16 ms with 6-V applied voltage, respectively. Apparently, the effect of director tilt deformation near the interdigital electrode side regions becomes more and more evident as the time changes from 4 to 16 ms. The director twist deformation effect in the inter-electrode regions also shows the same tendency. The transmittance dependence on different x positions at 4, 8, 12, and 16 ms are plotted in Fig. 7. At $t = 16$ ms, the transmittance in the curve almost reaches the maximum value which is 35% under real crossed polarizers. Due to the structure symmetry, the directors in the regions above each electrode's surface have little twist in response to the electric fields at different times, which results in dark regions above the electrodes. From Fig. 7, our simulation results agree well with those obtained from 2dimMOS, which indicates our derivations are dependable.

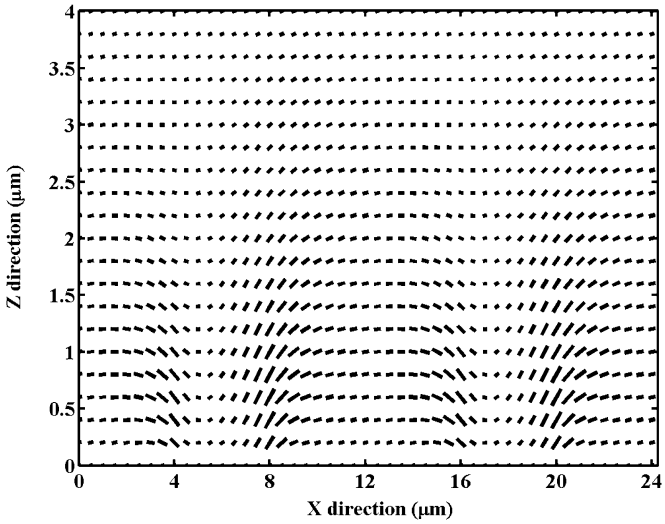

(a)

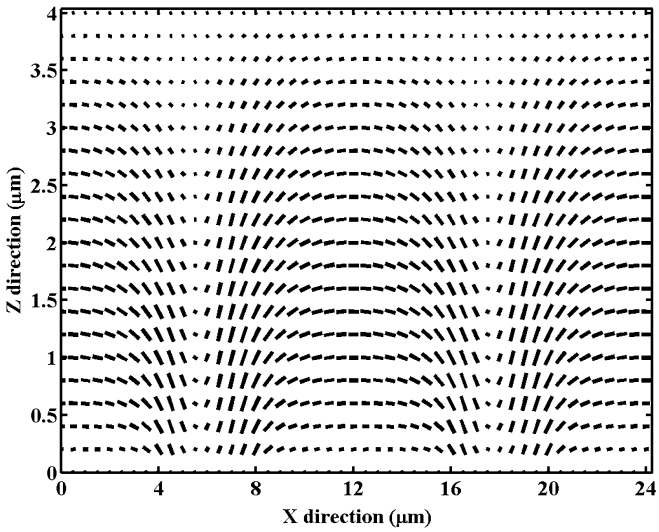

(b)

Fig. 6. (a) LC director distribution at 4 ms with 6-V applied. (b) LC director distribution at 16 ms with 6 V applied.

B. Three-Dimensional Super IPS Structure

The super IPS structure with zigzag electrodes is then studied by both derived FEM and FDM. The electrode shape and dimension in the bottom x-y plane are depicted in Fig. 8. And the cross-section view of the cell in x-z plane is same as Fig. 5. In our simulation, same LC material and cell gap as the 2-D simulation is taken in this configuration. The pretilt angles of LC directors are 2° from the x-y plane, and the rubbing angles are 90° away from the x axis in the x-y plane. Six volts are applied on the left electrode, while the right one is grounded to 0 V. The LC directors on the vertical boundaries (in z direction) are assumed to be strongly anchored in our simulations. Fig. 8 only shows a single period of the electrode structure within a pixel. The periodic boundary conditions in the lateral directions (both in x and y directions) are employed in both potential and LC director calculations.

Fig. 9(a) and (b) shows the cross-section view of the potential and director distributions at $t = 15$ and 60 ms, respectively. In sampling the cross-section view of x-y plane, the z is taken at $z = 3$ μm, and $y = 4$ μm is taken for the sampling of x-z cross-section view. As can be seen from these figures, the LC directors in the regions between the electrodes have been driven to the parallel direction of electric fields in these regions at $t = 15$ ms, and in these regions not much difference is observed for $t = 15$ ms and $t = 60$ ms. However, it takes a long time for the directors in the regions above the electrode surfaces to be fully rotated, as seen from $t = 15$ ms [see Fig. 9(a) and (b)] and $t = 60$ ms [see Fig. 10(a) and (b)]. This is because the electric field lines above the electrodes are more vertically distributed (z direction), while the electric fields in the inter-electrode regions are mostly along the horizontal direction. Similarly as in the 2-D case, the less rotation in these regions generates dark regions as illustrated in Fig. 11(a)–(c).

Fig. 11(a) to (c) shows the transmittance patterns at different time steps of $t = 15$, 25, and 60 ms from the derived FEM (top) and FDM (bottom). It can be seen that these two methods generate almost the same transmittance patterns. The main discrepancy of these two method comes from the center positions of electrodes (at $y = 16$ μm), where the electrode angle is very

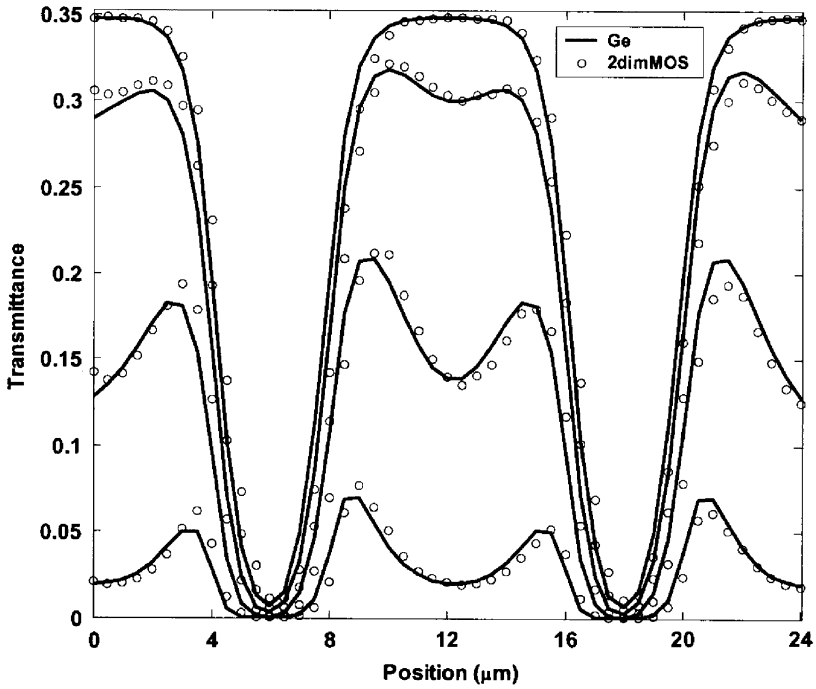

Fig. 7. Transmittance versus position at time equal to 4, 8, 12, and 16 ms from the derived FEM based method and the 2dimMOS.

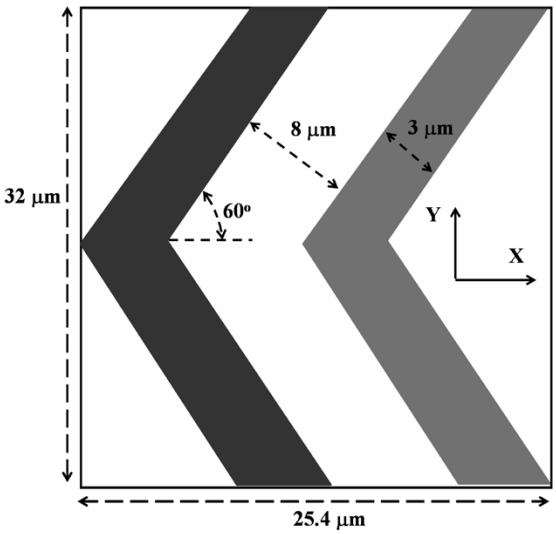

Fig. 8. Super IPS structure with zigzag electrodes in simulation.

sharp. The FEM and FDM might generate different LC director orientations, i.e., at these positions the LC director might rotate either in the $-x$ direction or in the $+x$ direction. However, in other regions, the results of these two methods match well with each other. Both methods show that the vertically distributed electric fields above the electrodes make these regions have relative low transmittances. Here the asymmetric dark region patterns in the y direction originate from the 2° pretilt angle in the y-z plane.

In addition to IPS structure described above, the derived method is also applicable to other complex LCD structures, such as multidomain vertical alignment (MVA) [40] and patterned vertical alignment (PVA) [41] modes.

IV. Conclusion

We have derived a comprehensive dynamic LC director calculation model based on FEM. The vector represented LC director is calculated by iteration between the calculations of potential and director distributions. Weak form is introduced to simplify the derivation of director calculation formulations. Excellent agreement is obtained between this method and the commercial 2dimMOS software in calculating a 2-D IPS structure. Our method is also validated by the comparison between FEM and FDM in simulating a 3-D super IPS structure, in which good agreement is obtained. The derived method is also applicable to other complex LC device designs and optimizations thereafter.

Appendix A
FEM Implementation for Director Update via Galerkin's Method

FEM is employed to get the solutions for the matrix A and vector b discussed in Sections II-B1. In FEM theory, a study domain Ω can be divided into M element domains with N nodes. In each element domain, there are m nodes with m interpolation functions (considering first-order interpolation functions) as well. In any element domain (e.g., eth element) the local director value n_l^e can be interpolated by its m local node values using m local basis functions as

$$\tilde{n}_l^e = \sum_{i=1}^{m} n_{l,i}^e W_i^e \quad (l = x, y, z) \tag{A-1}$$

where $n_{l,i}^e$ and W_i^e are the ith node value and interpolation function in the eth local element, respectively. The form of W_i^e is

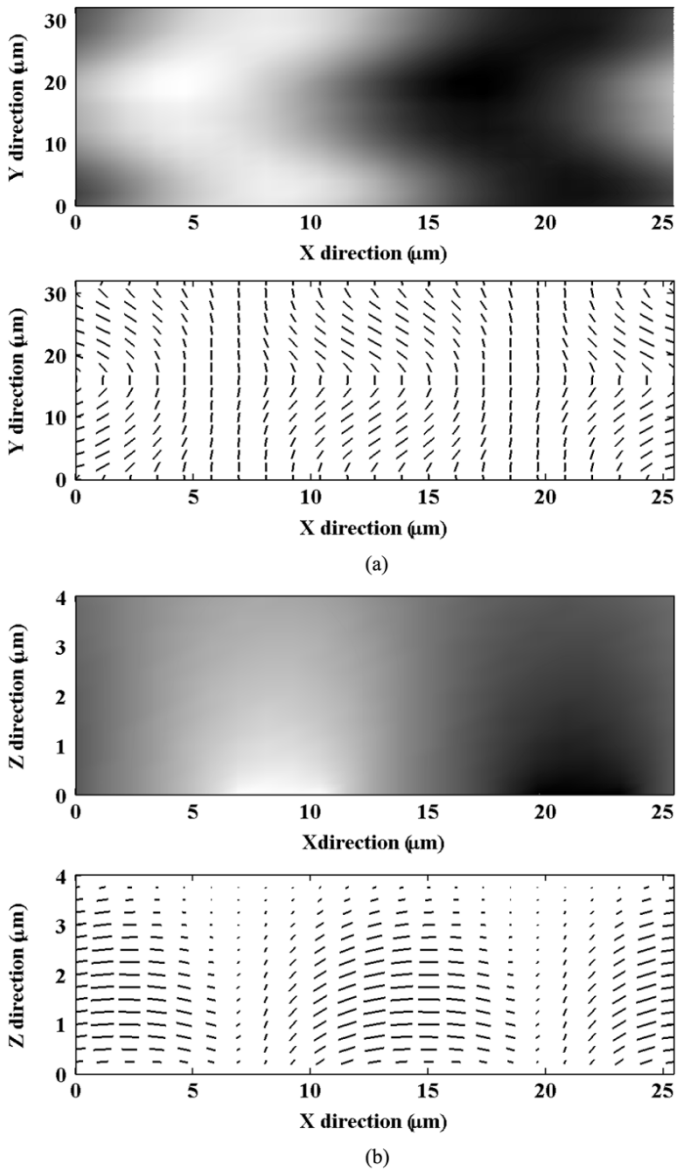

Fig. 9. (a) LC potential (top figure) and director (bottom figure) distributions in x-y plane at $z = 3$ μm at $t = 15$ ms with 6 V. (b) LC potential (top figure) and director (bottom figure) distributions in x-z plane at $y = 4$ μm at $t = 15$ ms with 6 V.

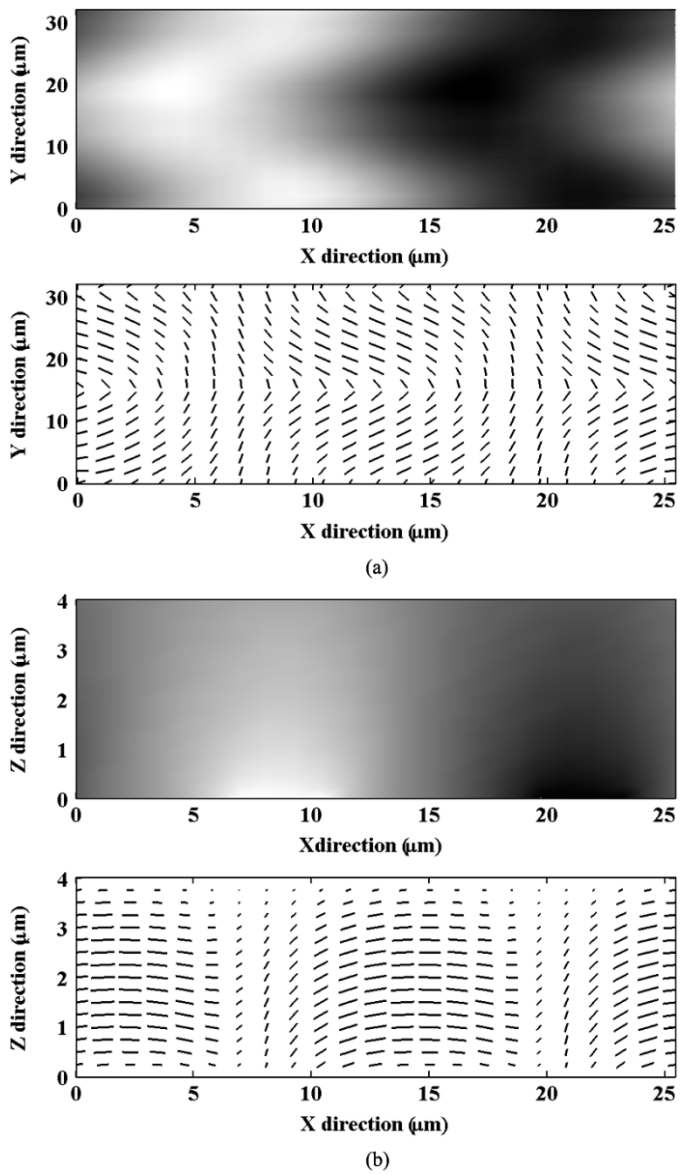

Fig. 10. (a) LC potential (top figure) and director (bottom figure) distributions in x-y plane at $z = 3$ μm at $t = 60$ ms with 6 V. (b) LC potential (top figure) and director (bottom figure) distributions in x-z plane at $y = 4$ μm at $t = 60$ ms with 6 V.

well-defined. For example, the first-order basis function in a 3-D tetrahedral element would be

$$W_i^e(x,y,z) = a_i^e + b_i^e x + c_i^e y + d_i^e z, \qquad (i = 1,2,\ldots m). \tag{A-2}$$

The coefficients a_i^e, b_i^e, c_i^e, and d_i^e can be determined by the node coordinate values and the volume of the tetrahedron [3], [4]. Detailed expressions of these coefficients are provided in Appendix C. Similarly, the residual R^e in each element domain Ω^e can be weighted by the element basis function as

$$\int_{\Omega^e} \left(\frac{d\tilde{n}_l^e}{dt} + \frac{1}{\gamma}[f]_{\tilde{n}_l}^e \right) W_i^e d\Omega^e = 0 \qquad (i = 1,2,\ldots m \text{ and } l = x,y,z). \tag{A-3}$$

Substituting the $\tilde{n}_l^e$ and expanding the above equation with a time-difference scheme leads to

$$(n_l^e)^{t+\Delta t} = (n_l^e)^t + \Delta t[A^e]^{-1}(b^e), \qquad (l = x,y,z) \tag{A-4}$$

where

$$A_{i,j}^e = \int_{\Omega^e} W_i^e W_j^e d\Omega^e \tag{A-5}$$

and

$$b_i^e = -\int_{\Omega^e} \frac{1}{\gamma}[f]_{\tilde{n}_l}^e W_i^e d\Omega^e. \tag{A-6}$$

By applying the assembling process of typical FEM procedure, the global matrix A and global vector b in (13) can be obtained from the element matrix A^e and element vector b^e.

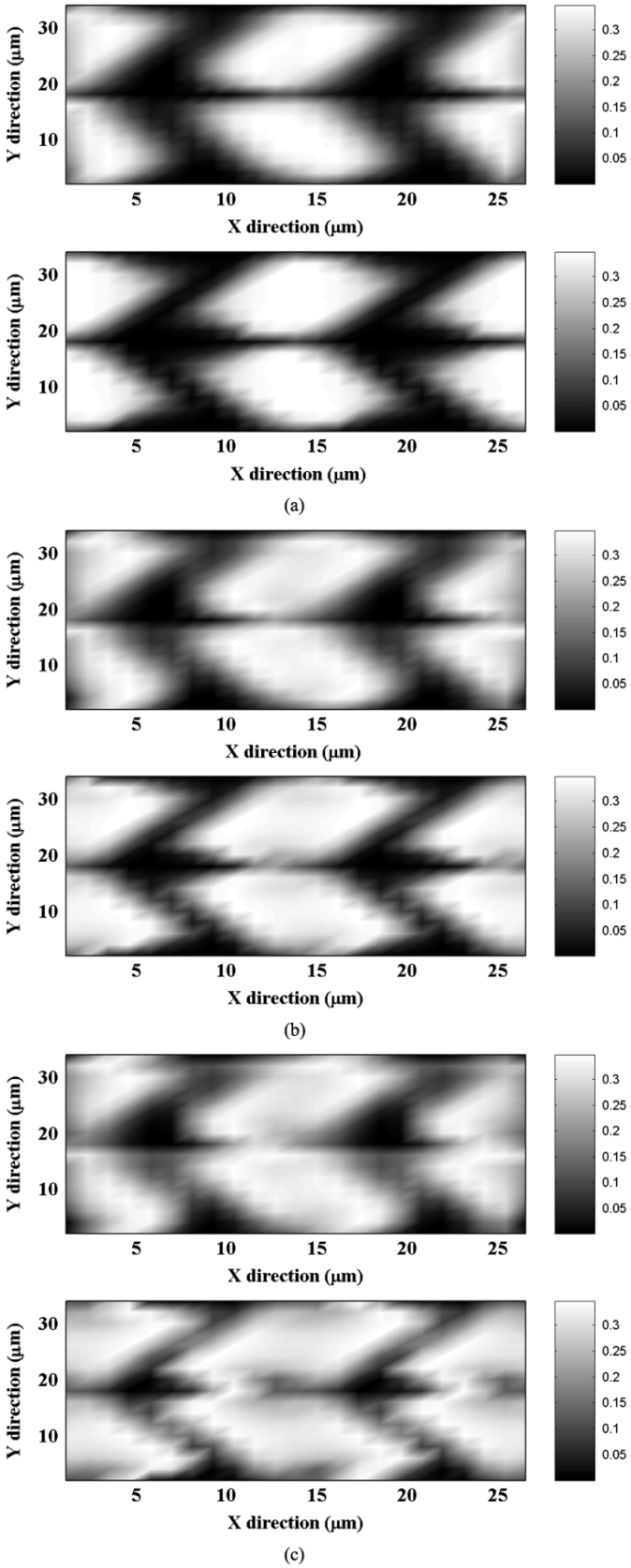

Fig. 11. (a) Transmittance pattern in the x-y plane by FEM (top figure) and FDM (bottom figure) at $t = 15$ ms with 6 V. (b) The transmittance patterns in the x-y plane by FEM (top figure) and FDM (bottom figure) at $t = 25$ ms with 6 V. (c) The transmittance pattern in the x-y plane by FEM (top figure) and FDM (bottom figure) at $t = 60$ ms with 6 V.

Appendix B
FEM Implementation for Potential Update via Ritz's Method

To derive the definite form of the matrix B in Sections II-B.2, we first express the electric field $\mathbf{E}$ into a vector form as

$$\mathbf{E} = -\left(\frac{\partial\Phi}{\partial x}, \frac{\partial\Phi}{\partial y}, \frac{\partial\Phi}{\partial z}\right)^T. \tag{B-1}$$

Therefore, the free electric energy F_e in (17) can be further expanded to

$$F_e = \frac{1}{2}\varepsilon_0 \int_\Omega \left(\frac{\partial\Phi}{\partial x}, \frac{\partial\Phi}{\partial y}, \frac{\partial\Phi}{\partial z}\right)\left(\overleftrightarrow{\varepsilon}\left(\frac{\partial\Phi}{\partial x}, \frac{\partial\Phi}{\partial y}, \frac{\partial\Phi}{\partial z}\right)^T\right) d\Omega. \tag{B-2}$$

A detailed check of F_e form reveals that it is a quadratic function of the Φ's spatial derivative. Therefore once the $\tilde{\Phi}$ in (18) is substituted in (19), the derivative of F_e with respect to Φ_i can be achieved by differentiation by parts

$$\begin{aligned}\frac{\partial F_e}{\partial \Phi_i} = {} & \frac{1}{2}\varepsilon_0 \int_\Omega \left(\frac{\partial W_i}{\partial x}, \frac{\partial W_i}{\partial y}, \frac{\partial W_i}{\partial z}\right) \\ & \times \left(\overleftrightarrow{\varepsilon}\left(\frac{\partial\Phi}{\partial x}, \frac{\partial\Phi}{\partial y}, \frac{\partial\Phi}{\partial z}\right)^T\right) d\Omega \\ & + \frac{1}{2}\varepsilon_0 \int_\Omega \left(\frac{\partial\Phi}{\partial x}, \frac{\partial\Phi}{\partial y}, \frac{\partial\Phi}{\partial z}\right) \\ & \times \left(\overleftrightarrow{\varepsilon}\left(\frac{\partial W_i}{\partial x}, \frac{\partial W_i}{\partial y}, \frac{\partial W_i}{\partial z}\right)^T\right) d\Omega \\ & (i = 1, 2, \ldots N).\end{aligned} \tag{B-3}$$

From above equation, each element $B_{i,j}$ of matrix B in (20) can be obtained by differentiating the (B-3) with respect to Φ_j

$$B_{i,j} = \frac{\partial^2 F_e}{\partial\Phi_i \partial\Phi_j}, \qquad (i, j = 1, 2, \ldots N). \tag{B-4}$$

This will lead to the expression of (21), which can be uniquely defined by FEM as below.

By applying the similar mesh and derivation as discussed in the FEM implementation of director profile section, we can obtain the element matrix B^e for each element, which has m nodes and m basis functions. The $B^e_{i,j}$ can be written as

$$\begin{aligned}B^e_{i,j} = \frac{\partial^2 F^e_e}{\partial\Phi^e_i \partial\Phi^e_j} = {} & \frac{1}{2}\varepsilon_0 \int_{\Omega^e} \left(\frac{\partial W^e_i}{\partial x}, \frac{\partial W^e_i}{\partial y}, \frac{\partial W^e_i}{\partial z}\right) \\ & \times \left(\overleftrightarrow{\varepsilon}\left(\frac{\partial W^e_j}{\partial x}, \frac{\partial W^e_j}{\partial y}, \frac{\partial W^e_j}{\partial z}\right)^T\right) d\Omega^e \\ & + \frac{1}{2}\varepsilon_0 \int_{\Omega^e} \left(\frac{\partial W^e_j}{\partial x}, \frac{\partial W^e_j}{\partial y}, \frac{\partial W^e_j}{\partial z}\right) \\ & \times \left(\overleftrightarrow{\varepsilon}\left(\frac{\partial W^e_i}{\partial x}, \frac{\partial W^e_i}{\partial y}, \frac{\partial W^e_i}{\partial z}\right)^T\right) d\Omega^e \\ & (i, j = 1, 2, \ldots m).\end{aligned} \tag{B-5}$$

From the above equation, one can get a definite $B^e_{i,j}$ value once W^e_i and the coordinate values of the small local domain Ω^e are

specified, as illustrated in Appendix C. By applying the assembling process of FEM, the global matrix B can be obtained from the element matrix B^e.

APPENDIX C
FEM INTERPOLATION FUNCTIONS

The local element shape for 1-D to 3-D cases is shown in Fig. 4(a) to (c). For simplicity in the expression, we just neglect the superscript element index e for both the local coordinate values (x, y, z) and the local interpolation functions W, as compared to (x^e, y^e, z^e) and W^e.

For the 1-D case in Fig. 4(a), the first-order interpolation (or basis) function can be expressed as

$$W_1 = \frac{x_2 - x}{x_2 - x_1}, \qquad x_1 \le x \le x_2, \tag{C-1}$$

$$W_2 = \frac{x - x_1}{x_2 - x_1}, \qquad x_1 \le x \le x_2. \tag{C2}$$

These two interpolation functions equal zero out of the local region. As we can see that the W_i is equal to 1 on the ith node, and 0 on the other one.

For the 2-D triangle shaped first order interpolation (or basis) functions as shown in Fig. 4(b), they have the expression as

$$W_1 = \frac{\Delta_1}{\Delta}, \tag{C-3}$$

$$W_2 = \frac{\Delta_2}{\Delta}, \tag{C-4}$$

$$W_3 = \frac{\Delta_3}{\Delta} \tag{C5}$$

where Δ is the area of the triangle, which is equal to

$$\Delta = \frac{1}{2}\begin{vmatrix} 1 & x_1 & y_1 \\ 1 & x_2 & y_2 \\ 1 & x_3 & y_3 \end{vmatrix} \tag{C-6}$$

here $||$ denotes the determinant of the inside matrix. And Δ_1, Δ_2, and Δ_3 are equal to

$$\Delta_1 = \frac{1}{2}\begin{vmatrix} 1 & x & y \\ 1 & x_2 & y_2 \\ 1 & x_3 & y_3 \end{vmatrix}, \tag{C-7}$$

$$\Delta_2 = \frac{1}{2}\begin{vmatrix} 1 & x_1 & y_1 \\ 1 & x & y \\ 1 & x_3 & y_3 \end{vmatrix}, \tag{C-8}$$

$$\Delta_3 = \frac{1}{2}\begin{vmatrix} 1 & x_1 & y_1 \\ 1 & x_2 & y_2 \\ 1 & x & y \end{vmatrix}, \tag{C-9}$$

respectively. Here the interpolation function is equal to zero out of the triangular region.

For the 3-D tetrahedron shaped first-order interpolation (or basis) functions as shown in Fig. 4(c), they can be expressed as

$$W_1 = \frac{V_1}{V}, \tag{C-10}$$

$$W_2 = \frac{V_2}{V}, \tag{C-11}$$

$$W_3 = \frac{V_3}{V}, \tag{C-12}$$

$$W_4 = \frac{V_4}{V} \tag{C-13}$$

where V is the volume of the tetrahedron, which is equal to

$$V = \frac{1}{6}\begin{vmatrix} 1 & x_1 & y_1 & z_1 \\ 1 & x_2 & y_2 & z_2 \\ 1 & x_3 & y_3 & z_3 \\ 1 & x_4 & y_4 & z_4 \end{vmatrix} \tag{C-14}$$

and V_1, V_2, V_3, and V_4 are equal to

$$V_1 = \frac{1}{6}\begin{vmatrix} 1 & x & y & z \\ 1 & x_2 & y_2 & z_2 \\ 1 & x_3 & y_3 & z_3 \\ 1 & x_4 & y_4 & z_4 \end{vmatrix} \tag{C-15}$$

$$V_2 = \frac{1}{6}\begin{vmatrix} 1 & x_1 & y_1 & z_1 \\ 1 & x & y & z \\ 1 & x_3 & y_3 & z_3 \\ 1 & x_4 & y_4 & z_4 \end{vmatrix} \tag{C-16}$$

$$V_3 = \frac{1}{6}\begin{vmatrix} 1 & x_1 & y_1 & z_1 \\ 1 & x_2 & y_2 & z_2 \\ 1 & x & y & z \\ 1 & x_4 & y_4 & z_4 \end{vmatrix} \tag{C-17}$$

$$V_4 = \frac{1}{6}\begin{vmatrix} 1 & x_1 & y_1 & z_1 \\ 1 & x_2 & y_2 & z_2 \\ 1 & x_3 & y_3 & z_3 \\ 1 & x & y & z \end{vmatrix} \tag{C-18}$$

respectively. The interpolation function is equal to zero out of the tetrahedral region.

REFERENCES

[1] A. Taflove, *Computational Electrodynamics: The Finte-Difference Time-Domain Method*. Reading, MA: Artech House, 1995.

[2] J. E. Anderson, P. Watson, and P. J. Bos, *LC3D: Liquid Crystal Display 3-D Directory Simulator, Software and Technology Guide*. Reading, MA: Artech House, 1999.

[3] J. Jin, *The Finite Element Method in Electromagnetics*, 2nd ed. Piscataway, NJ: Wiley-IEEE Press, 2002.

[4] Y. W. Kwon and H. Bang, *The Finite Element Method Using MATLAB*. BocaRaon, FL: CRC Press, 2000.

[5] Autronic-MELCHERS GmbH [Online]. Available: http://www.autronic-melchers.com/index.htm

[6] [Online]. Available: http://www.shintech.jp/eng/index_e.html

[7] [Online]. Available: http://www.sanayisystem.com/introduction.html

[8] V. G. Chigrinov, H. S. Kwok, D. A. Yakovlev, G. V. Simonenko, and V. I. Tsoy, "Invited paper: LCD optimization and modeling," in *SID Symp. Dig.*, vol. 28.1, May 2004, pp. 982–985.

[9] LCQuest [Online]. Available: http://www.eng.ox.ac.uk/lcquest/

[10] J. B. Davies, S. E. Day, F. Di Pasquale, and F. A. Fernandez, "Finite-element modeling in 2-D of nematic liquid crystal structure," *Electron. Lett.*, vol. 32, pp. 582–583, Mar. 1996.

[11] F. Di Pasquale *et al.*, "Two-dimensional finite-element modeling of nematic liquid crystal devices for optical communications and displays," *IEEE J. Sel. Topics Quantum Electron.*, vol. 2, pp. 128–134, Apr./May 1996.

[12] F. A. Fernandez, S. E. Day, P. Trwoga, H. F. Deng, and R. James, "Three-dimensional modeling of liquid crystal display cells using finite elements," *Mol. Cryst. Liq. Cryst.*, vol. 375, pp. 291–299, 2002.

[13] F. A. Fernandez, H. F. Deng, and S. E. Day, "Dynamic modeling of liquid crystal display cells using a constant charge approach," *IEEE Trans. Magn.*, vol. 38, no. 2, pp. 821–824, Mar. 2002.

[14] H. J. Yoon, J. H. Lee, M. W. Choi, J. W. Kim, O. K. Kwon, and T. Won, "Comparison of numerical methods for analysis of liquid crystal cell: In-plane switching," in *SID Symp. Dig.*, vol. 50.1, May 2003, pp. 1378–1381.

[15] S. H. Yoon, C. S. Lee, S. I. Yoon, J. H. Lee, H. J. Yoon, M. W. Choi, J. W. Kim, and T. Won, "Three-dimensional numerical simulation for understanding the fringe field effect on the dynamic behavior of liquid crystal," *Mol. Cryst. Liq. Cryst.*, vol. 413, pp. 333/[2469]–343/[2479], 2004.
[16] I. A. Yao, J. J. Wu, and S. H. Chen, "Three-dimensional simulation of the homeotropic to planar transition in cholesteric liquid crystals using the finite elements method," *Jpn. J. Appl. Phys.*, vol. 43, pp. 705–708, Feb. 2004.
[17] R. B. Meyer, "Piezoelectric effects in liquid crystals," *Phys. Rev. Lett.*, vol. 22, pp. 918–921, 1969.
[18] P. G. De Gennes and J. Prost, *The Physics of Liquid Crystals*, 2nd ed. Oxford, U.K.: Oxford Science, 1993.
[19] M. Ohe and K. Kondo, "Electro-optical characteristics and switching behavior of the in-plane switching mode," *Appl. Phys. Lett.*, vol. 67, pp. 3895–3897, Oct. 1995.
[20] S. Endoh, M. Ohta, N. Konishi, and K. Kondo, "Advanced 18.1-inch diagonal super-TFT-LCD's with mega wide viewing angle and fast response speed of 20 ms," *IDW'99*, pp. 187–190, Dec. 1999.
[21] R. N. Thurston and D. W. Berreman, "Equilibrium and stability of liquid-crystal configurations in an electric fied," *J. Appl. Phys.*, vol. 52, pp. 508–509, Jan. 1981.
[22] D. W. Berreman, "Numerical modeling of twist nematic devices," *Phil. Trans. R. Soc. Lond.*, vol. A 309, pp. 203–216, 1983.
[23] G. Haas, S. Siebert, and D. A. Mlynski, "Simulation of inhomogeneous electric field effects in liquid crystal displays," in *Proc. 9th Int. Display Conference, Society for Information Display and Institute of Television Engineers of Japan*, vol. 89, 1989, p. 524.
[24] D. W. Berreman and S. Meiboom, "Tensor representation of Oseen-Frank strain energy in uniaxial cholesterics," *Phys. Rev. A*, vol. 30, pp. 1955–1959, Oct. 1984.
[25] S. Dickmann, J. Eschler, O. Cossalter, and D. A. Mlynski, "Simulation of LCD's including elastic anisotropy and inhomogeneous field," *SID Dig. Tech. Pap.*, vol. 24, pp. 638–641, May 1993.
[26] H. Mori, E. C. Gartland Jr., J. R. Kelly, and P. J. Bos, "Multidimensional director modeling using the Q tensor representation in a liquid crystal cell and its application to the π cell with patterned electrodes," *Jpn. J. Appl. Phys.*, vol. 38, pp. 135–146, Oct. 1999.
[27] C. W. Oseen, "The theory of liquid crystals," *Trans. Faraday Soc.*, vol. 29, pp. 883–???, 1933.
[28] F. C. Frank, "On the theory of liquid crystals," *Discuss. Faraday Soc.*, vol. 25, pp. 19–???, 1958.
[29] J. E. Anderson, C. Titus, P. Watson, and P. J. Bos, "Significant speed and stability increases in multi-dimensional director simulations," *SID Tech. Digest*, vol. 31, pp. 906–909, 2000.
[30] Maplesoft, a divison of Waterloo Maple, Inc. [Online]. Available: http://www.maplesoft.com
[31] A. Rapini and M. J. Papoular, "Distortion d'une lamelle nématique sous champ magnétique conditions d'ancrage aus parois," *J. Phys. Colloq.*, vol. 30, p. C4, 1969.
[32] D. Demus, J. Goddby, G. W. Gray, and H-W. Spiess, *Handbook of Liquid Crystal*, V. Vill, Ed: Wiley-VCH, 1998, vol. 1.
[33] P. Rudquist and S. T. Lagerwall, "On the flexoelectric effect in nematics," *Liq. Cryst.*, vol. 23, pp. 503–510, May 1997.
[34] A. Mazzulla and F. Ciuchi, "Optical determination of flexoelectric coefficients and surface polarization in a hybrid aligned nematic cell," *Phys. Rev. E*, vol. 64, p. 021708, July 2001.
[35] A. J. Davidson and N. J. Mottram, "Flexoelectric switching in bistable nematic device," *Phys. Rev. E*, vol. 65, p. 051710, May 2002.
[36] C. V. Brown and N. J. Mottram, "Influence of flexoelectricity above the nematic Fréedericksz transition," *Phys. Rev. E*, vol. 68, p. 031702, Sept. 2003.
[37] D. L. Cheung, S. J. Clark, and M. R. Wilson, "Calculation of flexoelectric coefficients for a nematic liquid crystal by atomistic simulation," *J. Chem. Phys.*, vol. 121, pp. 9131–9139, Nov. 2004.
[38] L. A. Parry-Jones and S. J. Elston, "Flexoelectric switching in zenithally bistable nematic device," *J. Appl. Phys.*, vol. 97, p. 093515, Apr. 2005.
[39] L. M. Blinov and V. G. Chigrinov, *Electrooptic Effects in Liquid Crystal Materials*. New York: Springer-Verlag, 1994.
[40] A. Takeda, S. Kataoka, T. Sasaki, H. Chida, H. Tsuda, K. Ohmuro, T. Sasabayashi, Y. Koike, and K. Okamoto, "A super-high image quality multi-domain vertical alignment LCD by new rubbing-less technology," *SID Tech. Dig.*, vol. 29, pp. 1077–1080, May 1998.
[41] K. H. Kim, K. H. Lee, S. B. Park, J. K. Song, S. N. Kim, and J. H. Souk, "Domain divided vertical alignment mode with optimized fringe field effect," in *Proc. 18th Int. Display Research Conf. (Asia Display'98)*, 1998, pp. 383–386.

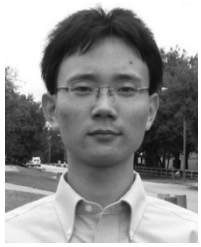

Zhibing Ge received the B.S. and M.S. degrees in electrical engineering from Zhejiang University, Hangzhou, China, and University of Central Florida, Orlando, in 2002 and 2004, respectively, and is currently working toward the Ph.D. degree at Department of Electrical and Computer Engineering, University of Central Florida, Orlando. His Ph.D. study concentration is in liquid crystal display modeling, transflective liquid crystal displays, and numerical analyses and optimization of liquid crystal devices.

Thomas X. Wu received the B.S.E.E. and M.S.E.E. degrees from the University of Science and Technology of China (USTC), Anhui, China, in 1988 and 1991, respectively, and the M.S. and Ph.D. degrees in electrical engineering from the University of Pennsylvania, Philadelphia, in 1997 and 1999, respectively.

From 1991 to 1995, he was with the faculty of the Department of Electrical Engineering and Information Science, USTC, as an Assistant and Lecturer. In Fall 1999, he joined the Department of Electrical and Computer Engineering, University of Central Florida (UCF), Orlando, as an Assistant Professor. His current research interests and projects include complex media, liquid crystal devices, electronic packaging of RF SAW devices, electrical machinery, magnetics and EMC/EMI in power electronics, chaotic electromagnetics, millimeter-wave circuits, and CMOS/BiCMOS RFICs.

Dr. Wu was awarded the Distinguished Researcher Award from the College of Engineering and Computer Science, University of Central Florida, in April 2004. Recently, he was listed in *Who's Who in Science and Engineering, Who's Who in America*, and *Who's Who in the World*.

Ruibo Lu received the M.S. degree in applied physics from Department of Physics, East China University of Science and Technology, Shanghai, China, in 1995, and the Ph.D. degree in optics from Department of Physics, Fudan University, Shanghai, China, in 1998. His research work for the Ph.D. degree focused on liquid crystal alignment and ferroelectric liquid crystal devices for display and advanced optical applications.

He was part of the faculty in Department of Physics, and later in Department of Optical Science and Engineering, Fudan University, Shanghai, China, from 1998 to 2001. He was an optical engineer in Lightwaves 2020 Inc., San Jose, CA, from 2001 to 2002. Since then, he joined the School of Optics/CREOL (now as College of Optics and Photonics), University of Central Florida, Orlando, as a research scientist. His research interests include liquid crystal display technology, wide viewing angle for liquid crystal TVs, liquid crystal components for optical communications and optical imaging using liquid crystal medium.

Xinyu Zhu received the B.S. degree from Jilin University, China, in 1996, and the Ph.D. degree from Changchun Institute of Optics, Fine Mechanics and Physics, Chinese Academy of Sciences, China in 2001. His Ph.D. research work involved mainly the reflective liquid crystal display with single polarizer.

He is currently a research scientist at the College of Optics and Photonics, University of Central Florida, Orlando. His current research interests include reflective and transflective liquid crystal displays, liquid-crystal-on-silicon projection display, wide view liquid crystal displays, and adaptive optics application with nematic liquid crystals.

Qi Hong received B.S. degree from the Nanjing University of Aeronautics and Astronautics, Nanjing, China, in 1992, and the M.S.E.E. degree from the University of Central Florida, Orlando, in 2002, where he is currently working toward the Ph.D. degree in the electrical engineering. His doctoral research topics include liquid crystal device modeling, wide viewing angle and fast response liquid crystal display.

He was design engineer at the Xiaxin Electronics Company Ltd., Xiamen, China, from 1992 to 2000.

Shin-Tson Wu (M'98–SM'99–F'04) received the B.S. degree in physics from National Taiwan University, and the Ph.D. degree from the University of Southern California, Los Angeles.

He is currently a PREP professor at College of Optics and Photonics, University of Central Florida (UCF), Orlando. Prior to joining UCF in 2001, he worked at Hughes Research Laboratories, Malibu, CA, for 18 years. His studies at UCF concentrate in foveated imaging, bio-photonics, optical communications, liquid crystal displays, and liquid crystal materials. He has co-authored two books: *Reflective Liquid Crystal Displays* (Wiley, 2001) and *Optics and Nonlinear Optics of Liquid Crystals* (World Scientific, 1993), four book chapters, and over 220 journal papers.

Dr. Wu is a Fellow of the IEEE, Society for Infformation Display (SID), and Optical Society of America (OSA).